Effect of Grain Boundary Characteristics on Intergranular Corrosion Resistance of 6061 Aluminum Alloy Extrusion

T. MINODA and H. YOSHIDA

The intergranular corrosion (IGC) behavior of 6061 aluminum alloy extrusions was investigated. After the IGC test in accordance with ISO/DIS 11846 (method B), heavy IGC was observed at the surface of the extrusion. However, little IGC occurred at the center plane of the extrusion thickness. It was considered that IGC was caused by the existence of precipitate-free zones (PFZs) because PFZs were clearly observed in the surface layer of the extrusion but were not clearly observed in the center position of the extrusion thickness. Furthermore, it was considered that the formation of PFZs was associated with the grain boundary characteristics. That is, most of the grain boundaries had random high angles in the surface layer of the extrusion, but 60 pct of the boundaries were lower than 0.26 rad (15 deg) in the center plane of the thickness. To verify this hypothesis, the center plane was cold rolled, recrystallized, and examined using the IGC test. As a result, heavy IGC was observed, while the center plane, in this case, had almost all random high-angle boundaries.

I. INTRODUCTION

THE extrusions of the 6061 aluminum alloy are widely used for structural components because of their good extrudability and relatively high strength. However, it is well known that copper addition to Al-Mg-Si alloys reduces their resistance to intergranular corrosion[1,2] limiting their use in corrosive environments such as at sea. By the way, the application of Al-Mg-Si alloys as automobile body sheets is increasing, and there are some reports about improvement in intergranular corrosion resistance of Al-Mg-Si-Cu alloys by controlling the artificial aging condition or lowering the corrosion potential by zinc addition.[1] For use as body sheets, solution heat treatments are carried out after cold rolling. On the other hand, most of the Al-Mg-Si alloy extrusions are produced by press quenching, which is a method of combining solution heat treatment and extrusion.[3] It is important to determine the behavior of Al-Mg-Si-Cu alloy extrusions with regard to intergranular corrosion because their microstructures are different from sheet materials.

In this study, the behavior of the 6061-T6 extrusions with regard to intergranular corrosion was investigated and the effect of the microstructures and grain boundary characteristics on the intergranular corrosion was discussed.

II. EXPERIMENTAL PROCEDURE

The 6061 aluminum alloy billet shown in Table I was prepared by direct chill casting with a diameter of 250 mm and then homogenized at 550 °C. After homogenization, the billet was heated to 520 °C for about 300 seconds using an induction heater and was extruded into the shape shown in Figure 1 at a speed of 133 mm/s. The extrusion was then press quenched with water. Artificial aging was carried out at 175 °C for 8 h.

T. MINODA, Research Engineer, and H. YOSHIDA, General Manager, are with the Research and Development Center, Sumitomo Light Metal Industries, Ltd., Nagoya 455-8670, Japan. Contact e-mail: tadashi__minoda@mail.sumitomo-lm.co.jp

Manuscript submitted July 9, 2001.

The 50 × 60-mm specimens for the intergranular corrosion tests were cut from the upper part of the extrusions. The intergranular corrosion tests were carried out in accordance with ISO/DIS 11846 (method B). The specimens were degreased with acetone and treated with mixed acid for surface preparation prior to the corrosion tests. After pretreatment, the specimens were immersed at room temperature in an aqueous solution containing 3 mass pct NaCl and 1 vol pct HCl. The corrosion tests were then carried out for 24 hours as the standard condition and 96 and 240 hours as the extended test periods. For the 96- and 240-hour tests, the solutions were renewed every 24 hours.

To clarify the differences in the intergranular corrosion behavior between the surface of the extrusions and the center thickness, the specimen was ground to half-thickness and polished with a #1200 abrasive paper, and then the intergranular corrosion test was carried out for 24 hours.

After the corrosion tests, the specimens were washed in water and the longitudinal-short transverse (L-ST) cross sections were observed. Furthermore, optical microstructures of the L-ST cross section before the corrosion tests were observed, the {111} pole figures of the longitudinal-long transverse (L-LT) cross sections were measured by the X-ray diffraction technique, and the grain boundary misorientation of the L-LT cross sections were measured using electron backscattered diffraction (EBSD) equipment with a scanning electron microscope (SEM). Moreover, the microstructures around the grain boundaries were observed using a JEM-200CX transmission electron microscope (TEM).

To identify the misorientation angle of the boundaries, which easily exhibit intergranular corrosion, a polished L-ST cross section of the extrusion underwent intergranular corrosion testing. After the test, the specimen was desmutted with concentrated nitric acid and etched with dilute HF solution, and the grain boundary misorientation angles were measured with an SEM with EBSD.

For the purpose of investigating the effect of decreasing low-angle boundaries on the intergranular corrosion behavior, two specimens of 6061-T4 extrusion after press quenching were ground to a 3-mm thickness. One specimen was cold rolled with a reduction of 25 pct and the other was not

Table I. Chemical Composition of 6061 Aluminum Alloy Extrusion (mass pct)

Si	Fe	Cu	Mn	Mg	Cr	Zn	Ti	Al
0.54	0.23	0.33	0.03	1.03	0.06	0.03	0.02	Bal.

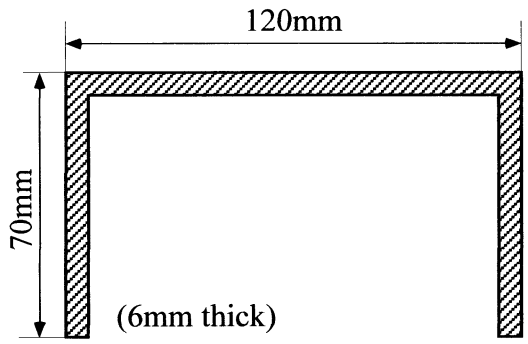

Fig. 1—Geometry of extruded section.

cold rolled. A solution heat treatment at 520 °C for 1 hour followed by quenching into water and artificial aging at 175 °C for 8 hours was then carried out on both specimens. These specimens next underwent intergranular corrosion testing measurement of the {111} pole figures, and observation of the optical microscope (OM) and TEM structures. Moreover, the grain boundary misorientation angles of the cold-rolled specimen after artificial aging were measured using the SEM with EBSD.

III. RESULTS AND DISCUSSION

A. *Intergranular Corrosion Behavior of the Extrusion*

Figure 2 shows the effect of the immersion time on the intergranular corrosion. Severe intergranular corrosion to a 300-μm depth occurred at 24 hours. However, the corrosion depth did not increase with time and then the corrosion propagated into the matrix for a long period. Figure 3 shows the results of the intergranular corrosion test with a specimen that was ground to half-thickness. Little intergranular corrosion was observed in Figure 3. These results show that the resistance to intergranular corrosion was different in the surface layer and inside the extrusion; that is, intergranular corrosion easily occurred in the surface layer, while it hardly occurred on the inside of the extrusion. Figure 4 shows the microstructures of the surface layer and the center of the extrusion. It seems that the amount of the precipitates in the surface layer and in the center of the extrusion is the same. Figure 5 shows the TEM micrographs and the selected area diffraction patterns of the precipitates. Both precipitates were identified as Mg_2Si. The amount of Mg_2Si precipitates is almost the same in the surface layer and in the center of the extrusion, and then the difference of the resistance to intergranular corrosion did not result from the distribution of the precipitates. Figure 6 shows the TEM micrographs of the specimen. Precipitate-free zones (PFZs) were clearly observed at most of the grain boundaries in the surface layer, while they were not clearly observed at most of the grain boundaries in the center of the specimen. Table II shows the electrode potentials of aluminum alloys.[4] The electrode

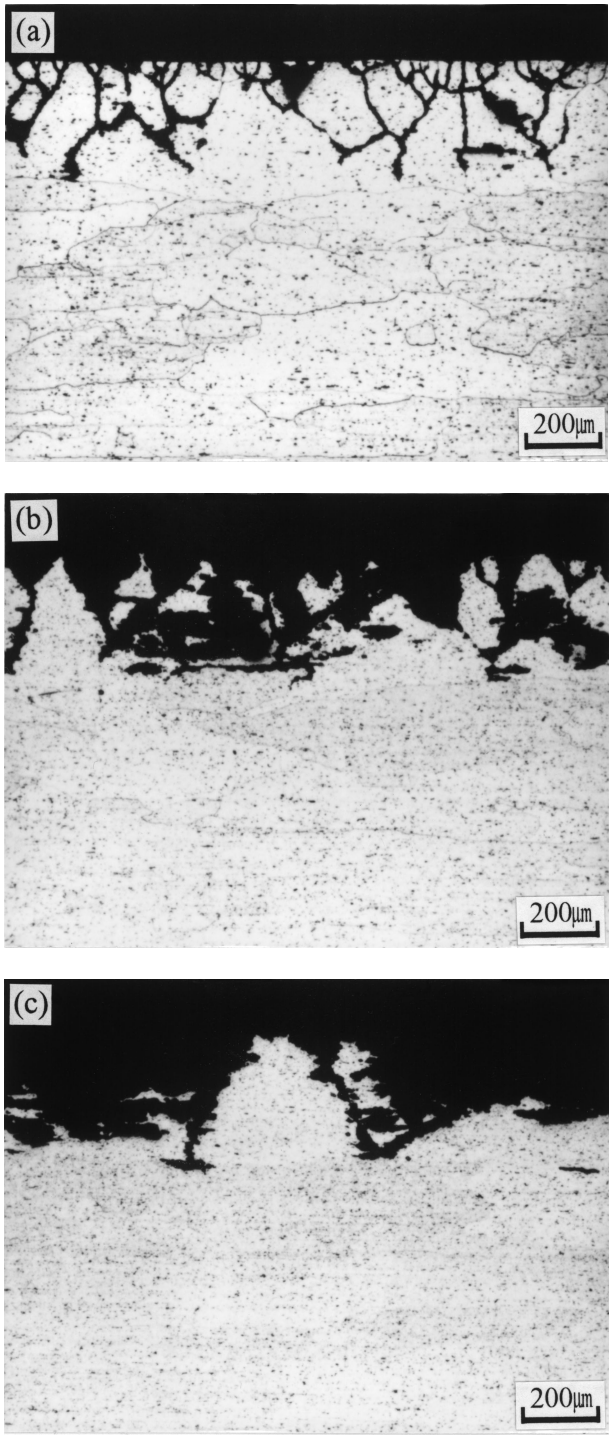

Fig. 2—Effect of immersed time on IGC. Specimens were immersed in an aqueous solution for (*a*) 24 h, (*b*) 96 h, and (*c*) 240 h.

potential of 6061-T4 alloy is the highest, that of T6 alloy is the second highest, and that of pure aluminum is the lowest in these three alloys. Because PFZs are solute-depleted zones, the electrode potential of PFZs is lower than that of the matrix. That is, the matrix with precipitates is more noble, while the PFZs are less noble in a peak-aged Al-Mg-Si-Cu alloy. In addition, the electrode potential of the Mg_2Si particle is higher than that of PFZs.[1] It is generally said that dissolution of the PFZs is due to the potential

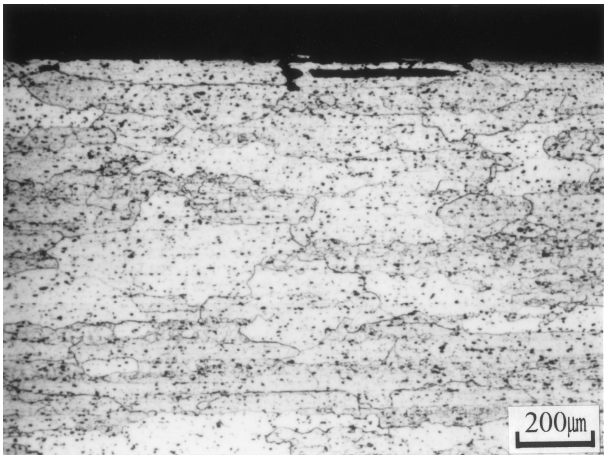

Fig. 3—Cross section of a specimen after an IGC test. The specimen was ground to half-thickness before the IGC test.

gap between the matrix, grain boundary precipitates, and PFZs.[1,5] For the 6061-T6 extrusions, it is considered that the electrode potentials of the matrix in the surface layer and the center of the extrusion are the same because the amount of Mg_2Si precipitates is the same, as shown in Figure 4. Then, the difference in the resistance to intergranular corrosion is due to the difference in PFZs. Intergranular corrosion easily occurred with anodic dissolution of the PFZs in the surface layer, because the PFZs were clearly observed in the surface layer. On the other hand, intergranular corrosion hardly occurred in the center layer of the extrusion because the PFZs were not clearly observed. Figure 7 shows the {111} pole figures of the L-LT cross sections. A random texture was observed at the surface, while a cube texture ($\{100\}\langle001\rangle$) was observed in the center layer. The maximum peak level was 3.5 at the surface and 22.5 at the center layer. Figure 8 shows the optical microstructures of the L-ST cross sections. The grains show a clear contrast in the surface layer of the extrusion, which is not observed at the center of the specimen. It appears that the recrystallized grains are present in the surface layer because shear stress and heat generation caused by the friction against the die bearing were greater than those inside the extrusion. Figure 9 shows the grain boundary misorientation of the extrusion. Most of the boundaries are higher than 0.26 rad (15 deg) at the surface, while 60 pct of the boundaries were lower than 0.26 rad (15 deg) at the center plane of the extrusion.

B. *Effect of Grain Boundary Characteristics*

The PFZs were clearly observed at most of the grain boundaries and intergranular corrosion easily occurred in the surface layer of the extrusion, while PFZs were not clearly observed at the most of the grain boundaries and intergranular corrosion did not easily occur inside the extrusion. In addition, most of the grain boundaries were high angle in the surface layer, while 60 pct of the grain boundaries were low angle inside the extrusion. By the way, it was reported that the grain boundary characteristics affect the nucleation and growth of the grain boundary precipitates in the Al-Zn-Mg alloy.[6] Furthermore, it is known that the weld decay of austenite stainless steel is caused by the chromium-depleted zones, which are caused by grain boundary

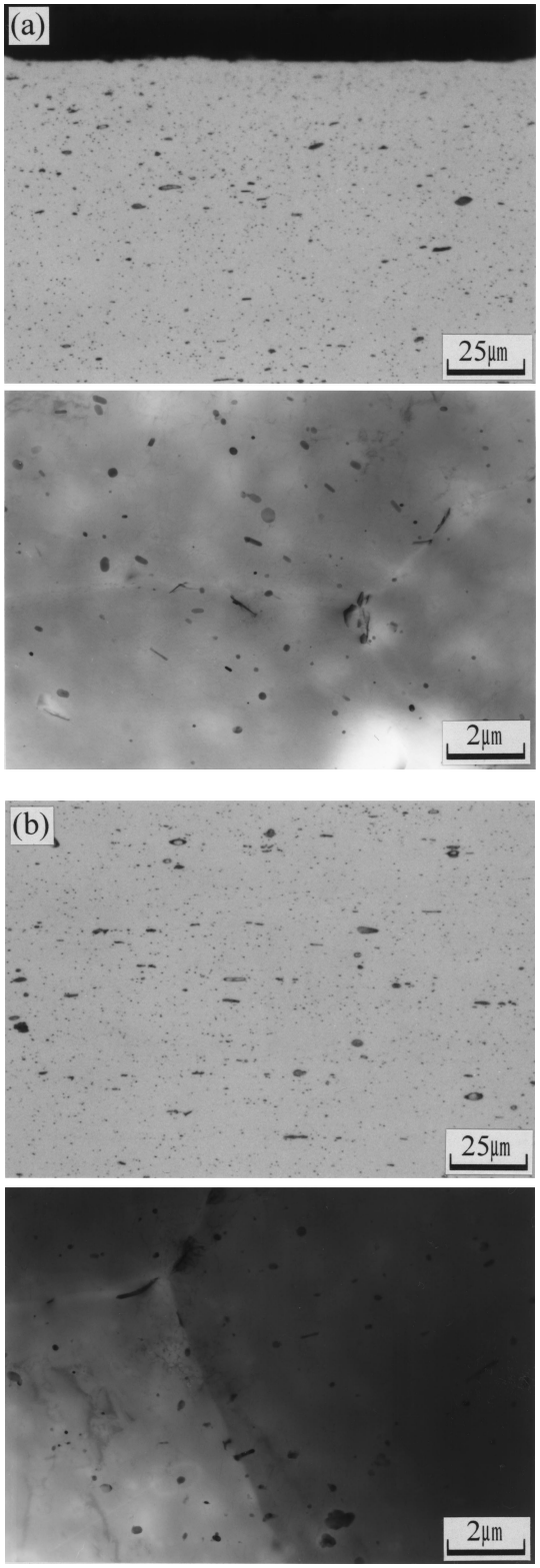

Fig. 4—OM and TEM structures of a 6061-T6 extrusion: (*a*) surface and (*b*) center of the sample.

precipitates of $Cr_{23}C_6$, and it is considered that the grain boundary characteristics affect the formation of the chromium-depleted zones. It was reported that the width of the chromium-depleted zones was smaller in coherent boundaries such as low-angle boundaries and coincidence cite

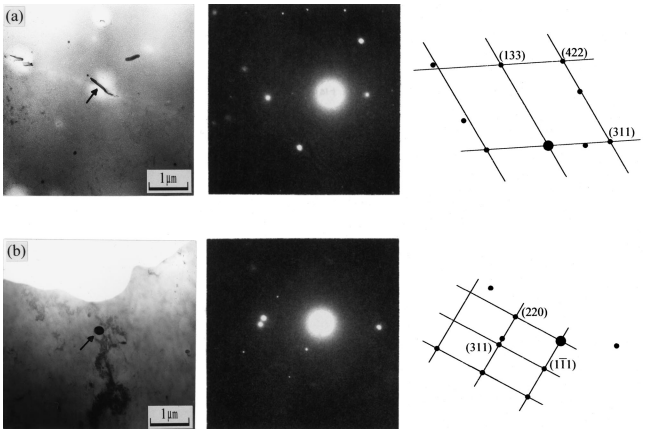

Fig. 5—TEM structures and the selected area diffraction patterns of the precipitates: (*a*) on the grain boundary and (*b*) in the matrix. Both precipitates were identified as Mg_2Si.

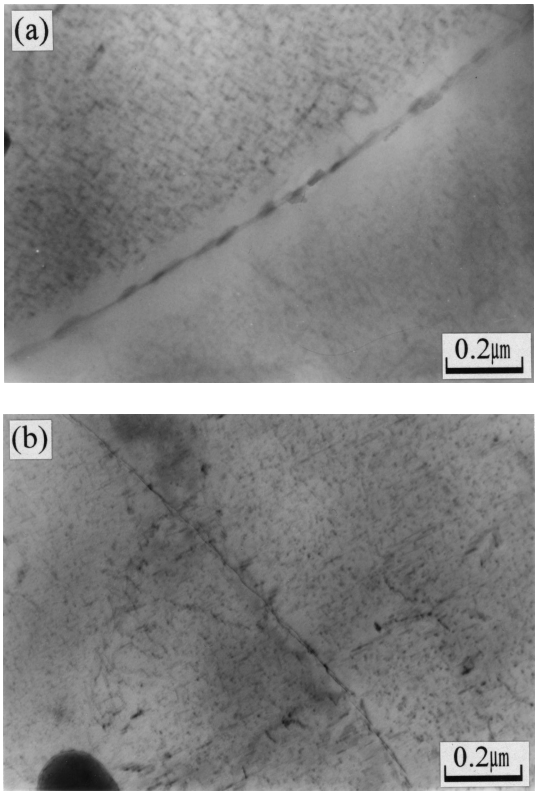

Fig. 6—TEM structures of a 6061-T6 extrusion: (*a*) surface and (*b*) center of the sample.

Table II. Electrode Potentials of Aluminum Alloys[4]

Alloy	Potential, *V**
99.95 Al	−0.85
6061-T6	−0.83
6061-T4	−0.80

*0.1 N calomel scale.

lattice (CSL) boundaries, while it was greater in random boundaries.[7] In general, it is said that the grain boundary

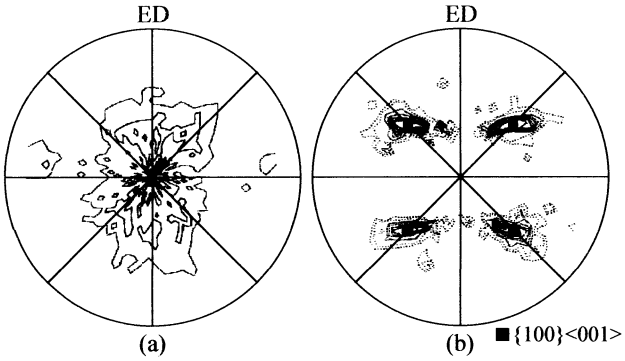

Fig. 7—{111} pole figures of a 6061-T6 extrusion: (*a*) surface and (*b*) center of the sample.

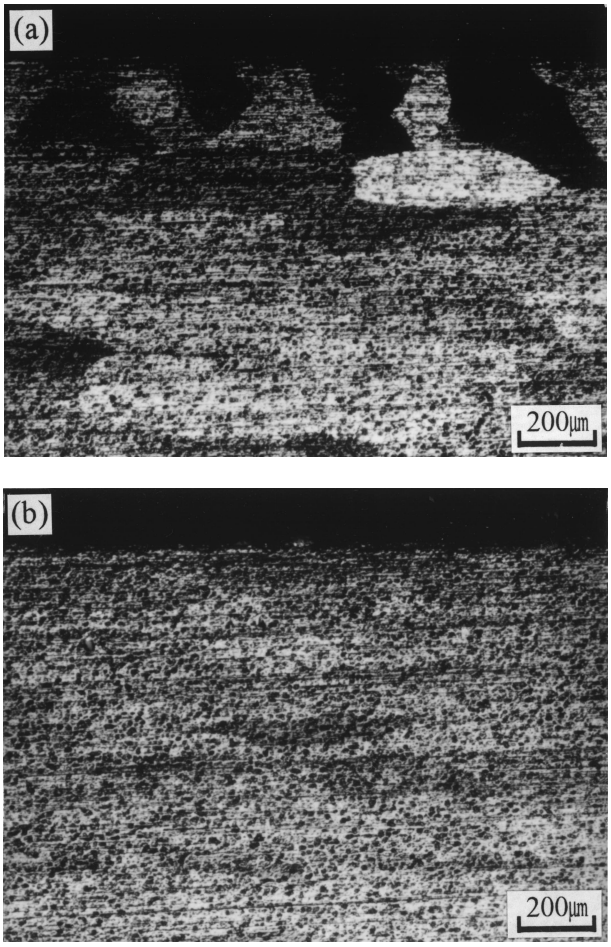

Fig. 8—Optical microstructure of L-ST cross section: (*a*) surface and (*b*) center of the sample.

energy is lower at coherent boundaries, while it is higher at incoherent boundaries.[8] Thus, it is considered that the amount of grain boundary precipitates changes with the difference in the grain boundary energy. It is suggested that grain boundary precipitates and PFZs easily form along random high-angle boundaries, while they hardly form along low-angle boundaries in 6061 extrusions as well as in stainless steel.

Figure 10 shows the optical microstructure of the L-ST cross section after the intergranular corrosion test and the

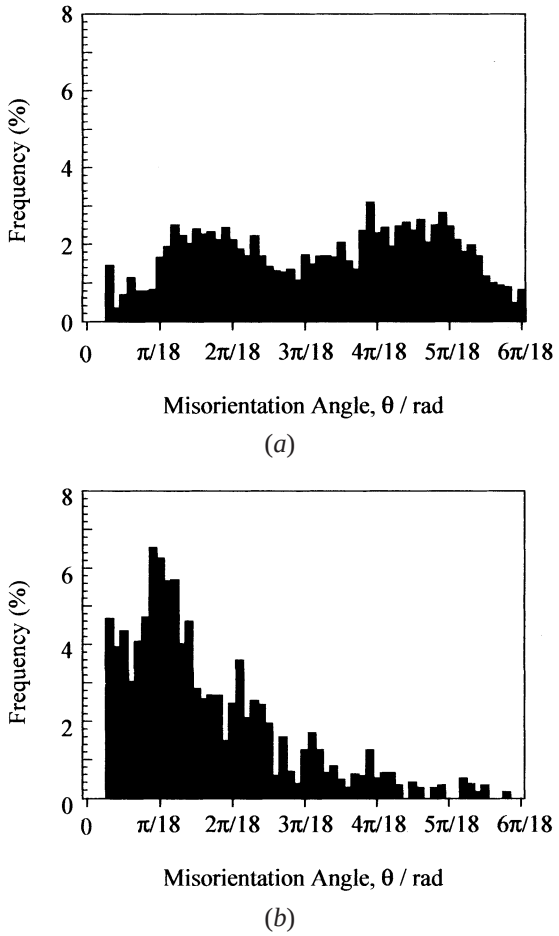

Fig. 9—Grain boundary misorientation angle distributions: (*a*) surface and (*b*) center of the sample.

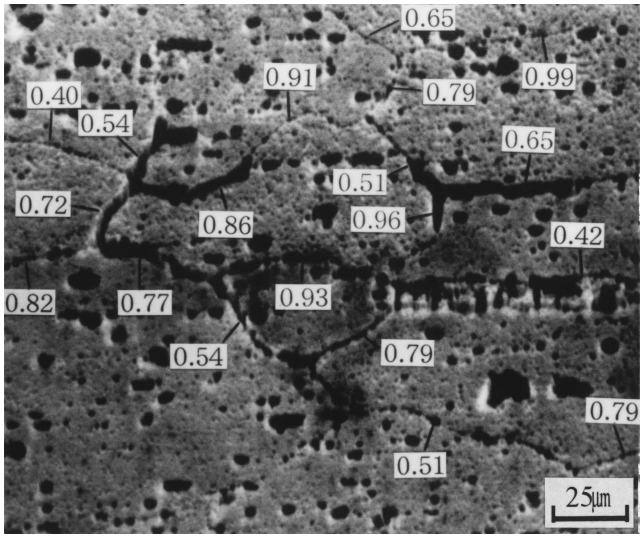

Fig. 10—Optical microstructure of the L-ST cross section after an IGC test. The numbers in this figure show the misorientation angle of the corroded boundaries (rad).

angles of the corroded boundaries. In addition, Figure 11 shows the misorientation angle distribution of the grain boundaries in which intergranular corrosion occurred. The angles of all the boundaries are greater than 0.26 rad

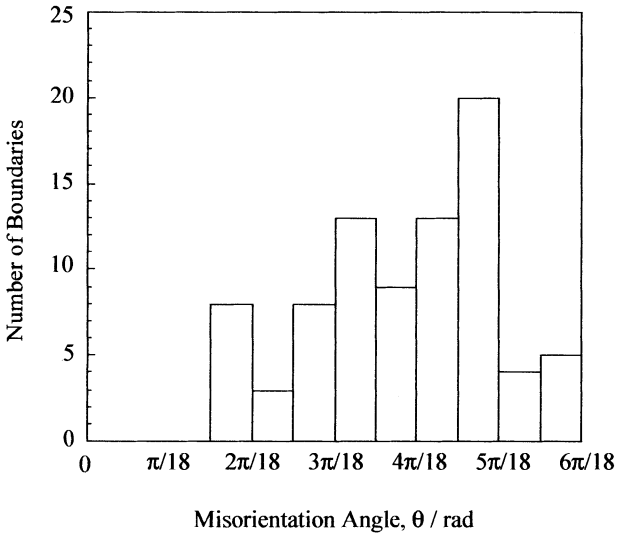

Fig. 11—Misorientation angle distribution of the grain boundaries in which intergranular corrosion occurred.

(15 deg), so the boundaries below 0.26 rad (15 deg) have a resistance to intergranular corrosion. Figure 12 shows the TEM structure of the grain boundaries and the Kikuchi lines from the grains. The misorientation angle is 0.40 rad in Figure 12(a), while it is 0.05 rad in Figure 12(b). Actually, it became clear that the misorientation of the grain boundary that did not show PFZ clearly had low angle. By the way, CSL boundaries also have a lower energy, like the low-angle boundaries. Especially, the lower Σ boundary has a lower energy; therefore, it is considered that intergranular corrosion does not easily occur in these boundaries. Actually, a previous study showed that the Σ3 boundaries have a resistance to stress corrosion cracking in austenitic alloys.[9] Table III shows the grain boundary characteristics and their rate in the surface layer and in the center of the specimen measured by EBSD. The rate of the Σ3 boundaries is only 1.4 pct in the surface layer and 0 pct in the center. Moreover, the Σ5-11 boundaries are only 3.1 pct in the surface layer and 2.7 pct in the center of the extrusion. Because the effect of CSL boundaries is very small, only low-angle boundaries can be taken into account in this study.

Figure 13 shows the distribution of high-angle boundaries (>0.26 rad) in the surface layer. Most of the high-angle boundaries connect with each other within 300-μm depth from the surface, while their connections are small over 300-μm depth. Then, it is considered that intergranular corrosion propagates easily in the surface layer because of the large connection of high-angle boundaries; however, it does not propagate more than 300-μm depth because of the small connection of high-angle boundaries.

C. *Intergranular Corrosion Behavior of Recrystallized Sample*

It became clear that intergranular corrosion did not easily occur due to the amount of low-angle boundaries; therefore, it is suggested that intergranular corrosion will easily occur even at the center of the sample where most of the grain boundaries have random high angles. Figure 14 shows the optical microstructures of the 6061 extrusion after grinding

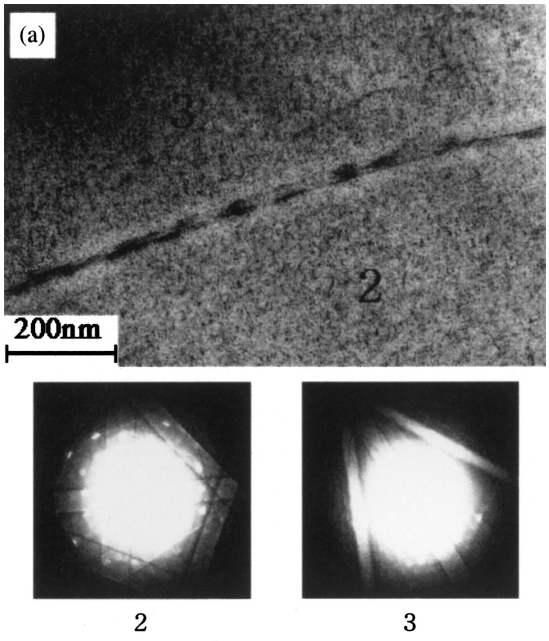

Fig. 12—TEM structures of the grain boundaries and the Kikuchi lines from the grains: (*a*) PFZ is observed clearly and (*b*) PFZ is not observed clearly.

Table III. Grain Boundary Characteristics and Their Ratios Measured by EBSD

Type of Boundary	Surface Layer	Center
Low angle*	18.3 pct	59.8 pct
Σ3	1.4 pct	0 pct
Σ5-11	3.1 pct	2.7 pct
Random	77.2 pct	37.5 pct

*Below 0.26 rad.

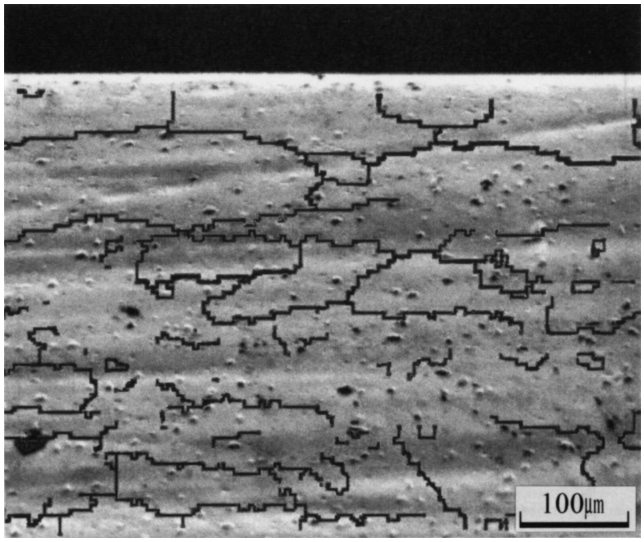

Fig. 13—L-ST cross section in the surface layer of the extrusion. The lines show the high-angle boundaries with more than 0.26 rad.

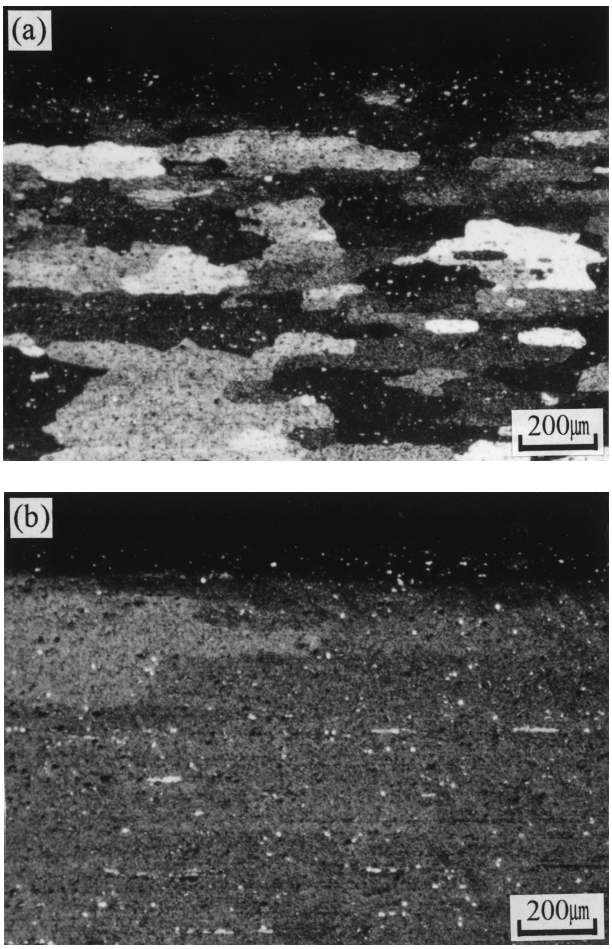

Fig. 14—Effect of the reduction of cold rolling on the recrystallized grains after cold rolling, solution heat treatment, and artificial aging. The reductions in cold rolling were (*a*) 30 pct and (*b*) 0 pct.

to half-thickness, polishing, cold rolling, solution heat treatment, and artificial aging. For the specimen without cold rolling in Figure 14(b), the grains still show an indistinct

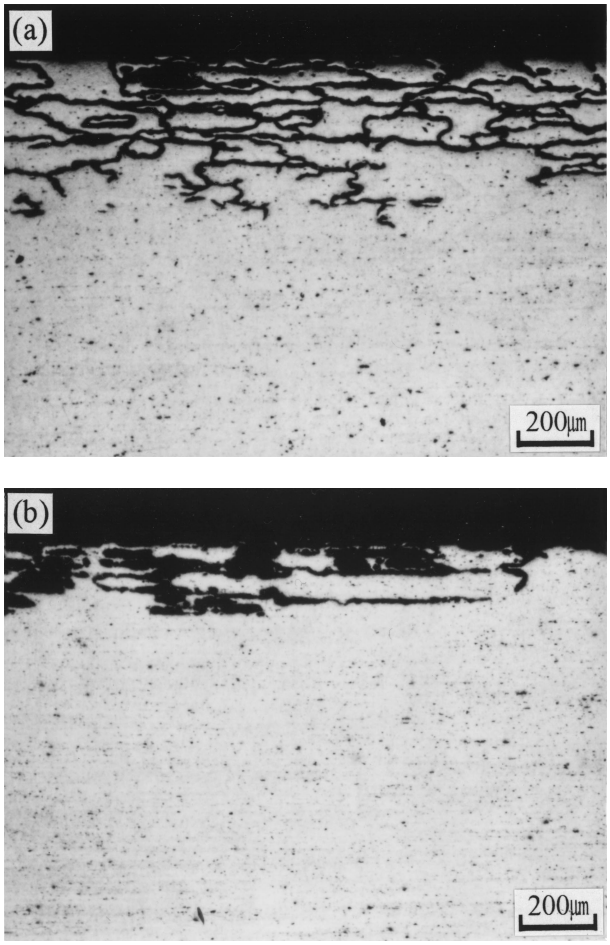

Fig. 15—Cross section of recrystallized specimens after the IGC test. The reductions in cold rolling before solution heat treatment were (*a*) 30 pct and (*b*) 0 pct.

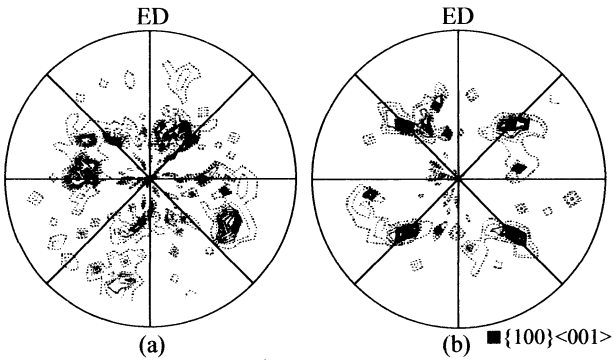

Fig. 16—{111} pole figures of recrystallized specimens. The reductions in cold rolling before solution heat treatment were (*a*) 30 pct and (*b*) 0 pct.

contrast. However, for the cold-rolled specimen in Figure 14(a), the grains show a clear contrast. Figure 15 shows the results of the intergranular corrosion tests. Intergranular corrosion was only slightly observed in the specimen without cold rolling, while heavy intergranular corrosion was observed in the cold-rolled specimen. The {111} pole figures of the specimens are shown in Figure 16. Cube and rotated cube textures were observed in the specimen without cold rolling in Figure 16(b). It is considered that the press-quenched specimen showed only the cube texture in the

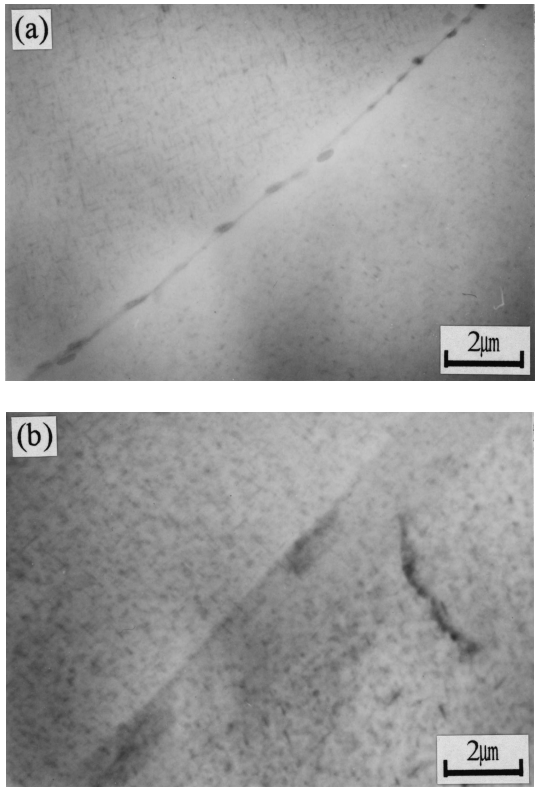

Fig. 17—TEM structures of recrystallized specimens. The reductions in cold rolling before solution heat treatment were (*a*) 30 pct and (*b*) 0 pct.

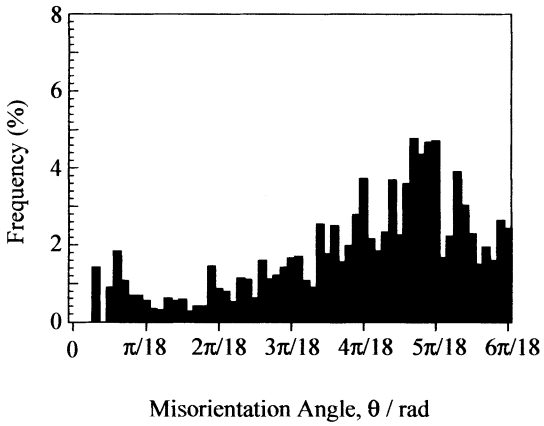

Fig. 18—Grain boundary misorientation angle distribution of the cold-rolled and recrystallized specimen after artificial aging.

center of the sample, as shown in Figure 7(b), because the time between the extrusion and quenching was so short that the specimen was quenched during recrystallization. Therefore, the rotation of grains from the cube texture occurred during the solution heat treatment. The random high-angle boundaries then increased and intergranular corrosion easily occurred. On the other hand, the grains were randomly oriented in the cold-rolled specimen. Figure 17 shows the TEM micrographs. The PFZs were not clearly observed in the specimen without cold rolling in Figure 17(b), while they were clearly observed in the cold-rolled specimen in Figure 17(a). Figure 18 shows the grain boundary misorientation angle distribution of the cold-rolled specimen after artificial aging. Most of the boundaries were higher

than 0.26 rad (15 deg). Therefore, it became clear that the grain boundary characteristics affect the formation of the PFZs in the 6061 extrusions.

IV. CONCLUSIONS

1. The intergranular corrosion test of the 6061-T6 extrusion indicated that severe intergranular corrosion to a 300-μm depth occurred at 24 hours. However, the corrosion depth did not increase with time and then the corrosion propagated into the matrix for a long period.
2. The PFZs were clearly observed at the surface layer, while they were not clearly observed in the center of the sample. It is apparent that the dissolution of the PFZs occurs during the intergranular corrosion test because of the potential gap between the matrix, grain boundary precipitates, and PFZs.
3. Most of the boundaries were higher than 0.26 rad (15 deg) in the surface layer, while 60 pct of the grain boundaries were lower than 0.26 rad (15 deg) in the inside of the extrusion.
4. It was concluded that the PFZs accelerate intergranular corrosion, and the grain boundary characteristics affect the formation of the grain boundary precipitates and PFZs. Intergranular corrosion easily occurs at a random high-angle boundary, where grain boundary precipitates and PFZs easily form, while intergranular corrosion does not easily occur at the low-angle boundaries, where grain boundary precipitates and PFZs are rare.

ACKNOWLEDGMENTS

The authors acknowledge Professor Z. Horita, Kyushu University in Japan, for the measurements of the grain boundary misorientations by Kikuchi-lines of TEM structures. Thanks are also due to Professors K. Ikeda, K. Maruyama, and H. Kokawa, Tohoku University in Japan, for valuable discussions.

REFERENCES

1. K. Yamaguchi and K. Tohma: *Proc. 6th Int Conf. on Aluminum Alloys*, T. Sato, S. Kumai, T. Kobayashi, and Y. Murakami, eds., The Japan Institute of Light Metals, Tokyo, 1998, pp. 1657-62.
2. M. Bloeck and J. Timm: *Aluminium*, 1994, vol. 70, pp. 87-92.
3. T. Sheppard: *Extrusion of Aluminium Alloys*, Kluwer Academic Publishers, Hingham, MA, 1999, pp. 186-98.
4. Kent R. Van Horn: *Aluminum Vol. I, Properties, Physical Metallurgy and Phase Diagrams*, ASM, Cleveland, OH, 1967, vol. 210, p. 212.
5. R. Dif, D. Bechet, T. Warner, and H. Ribes: *Proc. 6th Int Conf. on Aluminum Alloys*, T. Sato, S. Kumai, T. Kobayashi, and Y. Murakami, eds., The Japan Institute of Light Metals, Tokyo, 1998, pp. 1991-96.
6. P. Czurratis, R. Kroggel, and H. Loffler: *Z. Metallkd.*, 1988, vol. 79, pp. 307-12.
7. H. Kokawa: *Mater. Jpn.*, 1996, vol. 35, pp. 655-62.
8. F.J. Humphreys and M. Hatherly: *Recrystallization and Related Annealing Phenomena*, Pergamon, Elmsford, NY, 1996, pp. 57-83.
9. V.Y. Gertsman and S.M. Bruemmer: *Acta Mater.*, 2001, vol. 49, pp. 1589-98.